Success criterion derivation for the swarm satellite application of pulsed superconductive solenoids in freight transport

Morgan Wegener [1]

[1]H. Industries

October 30, 2023

Abstract

A thought experiment on the effect of the central yoke rod in a superconductive solenoid and the resulting induction and repulsive effect on a steel plate placed above the solenoid is explored with an analytical derivation using equations from various literature sources. A review of the current design thinking in pulsed solenoids is presented before a sample design is investigated through multiple scenarios.

11

Success criterion derivation for the swarm satellite application of pulsed superconductive solenoids in freight transport

M. J. Wegener

Abstract

Theoretically, high energy pulsed solenoids could be mounted in a satellite frame to deliver pulsed electromagnetic propulsion. A swarm of satellites arranged in a square pyramid is theorized to create a distributed propulsion method for freight transport. Multivector propulsion systems are used in boats with multiple propellers where the focal point of harmonized wave interaction imparts the maximum propulsion vector. Before modelling wave interactions and distributed inertial masses, the foundational theories of electromagnetism must be examined in context and a success criterion developed to indicate if the proposed design is capable of producing the required force against the object above's inertia. An analytical solution to an iron cored, thin solenoid interacting with a flat pancake solenoid is investigated with a proposed high energy pulse solenoid design. The force enhancement of the yoke rods higher relative permeability is found to be a field limited nonlinear multiplier that can be included in contextual electromagnetic equation derivations. This inclusion is investigated in design scenarios then discarded as it is one of two sources of large variance in electromagnetic results; the other being decomposition of the homogenous metal plate to a pancake coil equivalent resistance circuit. The success criterion is isolated from the formulae then compared to proposed requirements to assess viability. The reduction of the electromagnetic force formulation to a multiplier of the current induced in the object above forms a clear success criterion for design inspection of pulsed electromagnets in relation to the force required for the specified freight transport capacity.

INTRODUCTION

It is proposed that an analytical treatment of particle accelerator loops & high energy pulsed solenoid (HEPS) advancements can be applied to satellite orbital transfer manoeuvers with scaled designs propelling steel shipping containers. This translation of magnetic levitation (maglev) mechanics between two elliptical contexts is first considered geometrically to frame the problem before the method of action is inspected [25]. If the concept is able to be validated analytically, the system can then be built in MATLAB to publish research on design & manufacturing.

A satellite is stationary in its own orbital frame of reference, acting like a rail in comparison to the moving train overhead. When many are joined together in a tight knit swarm, the arrangement of geometries form the architectural components of larger, 'stationary', orbital structures. A flat, square grid array of satellites fitted with scaled HEPS creates a several meter area maglev launch platform. Each solenoid is capable of pulsing high strength electromagnetic field lines that expand as an ellipsoid, a 3D elliptical shape defined by the winding length and thickness of the magnetic coil [31]. A conductive object, such as a steel shipping container, placed directly above the array will be affected by multiple maglev pulse vectors, creating a larger net velocity by vector combination. The pulsed electromagnetic fields area of intercept is defined by the ellipsoid which intersects as a circle on the XY plane in the object above's surface. This circle is the area of induction affected by the pulsed electromagnetic field surface so is treated as an equivalent resistance circuit (ERC) of a single wire, also known as a pancake coil. This system of interactions will be framed analytically using a construction of multiple sources in respective areas to define the problem and it's bounds in electromagnetic theory and current research. Once the problem is defined, a success criterion is isolated to assess whether the solenoid designs inductive force generation exceeds the object above's inertia and propulsion is successful.

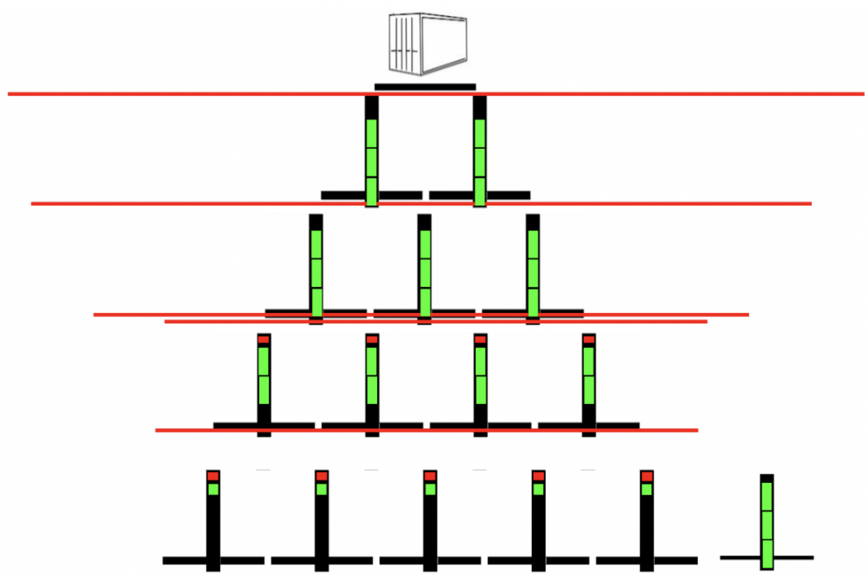

Fig. 1. Application of high energy pulsed solenoids with capacitor power supply in a satellite swarm.

Conceptually it is considered that the problem has two components, the foundational physics of multiple fields being wholly functional and the physical components functioning in the proposed orbital environment. Broad literature reviews have concluded that no singular aspect of context or design prevents function so the proposed concept must be viable by conclusion. The electromagnetic analysis of the proposed interaction is the purpose of this paper, component technologies are detailed before the design is assessed in relation to the problem.

Context

The vacuum of space is cold and causes no drag on propulsion or hindrance to electromagnetic fields, presenting advantageous operating conditions for distributed maglev propulsion. This problem is framed analytically in ideal conditions to isolate the interaction of one satellite to the object above. The mechanics of this interaction can be viewed in the Ring Launcher experiment where the maglev effect is demonstrated by propelling a small steel ring upwards from its original position sitting on top of a solenoid as current flows into the coil [3]. The calculated force required to lift the ring against gravity is compared to the force experienced between the applied and induced magnetic fields to determine if lift is achievable.

These mechanics are replicated in the satellite swarm, as each satellite's pulse acts as a ring launcher and each parallel layer acts as a flat plate pushing upwards from its position. In total, this system of parallel layers acts like the coils of a large spring. The swarm base layer must be held in a fixed orbital position requiring thruster offset during launch, however all forces are distributed across the electromagnetically XY tethered layers that act as combined inertial masses. In this context, the square arrangement of four satellites below each higher layer object and combination of the four pulse vectors generates a combination vector in the Z direction, at a tangent to the system's orbital arc. The objects centre of mass is then moved along the resultant sum of vectors by the net forces work. Application of the procedure in reverse would then be capable of decelerating payloads at the destination swarm. This novel propulsion method is not possible in single point thrust designs and is only functional in the advantageous orbital setting.

Satellite design is considered as a component size constraint, the operational limitations such as heat loss, solar absorption and orbital maintenance are beyond the scope of this paper. These factors and others will be addressed by modelling and research provided the electromagnetic problem construction, context and solution are valid. No further treatment is given to the orbital context as the electromagnetic interaction is the core problem to resolve and there is a wide variety of research available on the development and cutting edge of satellite componentry [4, 15, 38]. The satellite frame material selection determines the mechanical stress limits while power storage subcomponents establish the maximum power supply limit.

Literature on various material limits establish the boundary conditions of the problem and current design thinking establishes relative sizing of components within the satellites available volume [38]. Evaluation of the concept within the framework of material limits is sought by deriving a simple propulsion success criterion from the construction of the problem. Provided the foundational mechanics are valid, no material limits are exceeded and the success criterion is satisfied, the proposed design is theoretically capable of propelling a shipping container on an unpowered interorbital arc for arrival in an extraterrestrial orbit.

Superconductive Solenoid Design

A literature review on the current state of design is presented to define the proposed design and material limits to be assessed.

In 1911, the Dutch physicist H. Kamerlingh Onnes discovered the phenomenon of superconductivity, the vanishing of electrical resistance in some metals at very low (<10 K) temperatures. The discovery inspired Kamerlingh Onnes to propose a 100,000 Gauss (10 T) solenoid two years later based on a superconducting coil cooled with liquid helium, yet it took more than 50 years to realize this design in practice [61]. In 1989 Motokawa et al at Tohoku University built the first of a series of a new class of resistive magnet that were referred to as repeating pulsed magnet [43] which provided pulsed fields of a few millisecond duration as high as 25 T once every 2 second [8]. These repetitively pulsed magnets were first built in a solenoid configuration [44, 8, 21] Today, pioneering research is being conducted by several high magnetic field centres [13, 19] around the world which are achieving >100T strength fields and long pulse lengths.

Particle accelerators have used superconductive components for many years to achieve the required energy densities in size constrained tunnels underground [1, 31]. The superconductors allow current densities orders of magnitude greater than regular resistance conductive materials like copper [51]. Initially, small accelerators used strings of permanently active electromagnets to create a controlled turning path for particle beams but with developments in high energy pulsed electromagnetics across the past two decades this has changed [31, 51]. Development of high energy pulsed solenoids (HEPS) has allowed a series of timely pulses to turn the particle beams direction, reducing accelerator energy costs and rapidly advancing electromagnetic design and research [27, 31, 50, 51]. The progress in pulsed high magnetic field research in the last two decades was driven by the transition to multicoil superconductive solenoid designs [22] and capacitor power systems [18, 21, 24].

The addition of multiple concentric coils each pulsing as the successive outer coils are energised is the key [23] to reaching 100T fields and beyond [54]. The design improvements and high energy density components required to achieve such a field enables high quality, high power solenoids scaled to a small satellites capacitor system power output. A field of >100T is likely not required in the proposed contex. Magnet designers frequently trial improvements on 0.5m to 2m test coils [14, 41, 62] and a review of papers on small bore coils [13, 40] shows that high field pulses are achievable in a satellite deployable package. [8, 12] By using the highest current densities achievable, the solenoids pulsewave induces the strongest current in the object above and the induced field repulsion force is maximised as shown in Section IV.

As research has optimised NbTi cables almost to their material limits, Nb3Sn has seen increased development as the next generation substitute due to its higher temperature, field strength & current density capabilities [27]. Nb3Sn is superconductive below 18.1K with a maximum critical field strength of 25T, if the material exceeds either of these limits then a quench occurs where superconductivity is lost and the pulsed power must be diverted. Later research has refined the thermodynamic field strength surface that bounds the material's superconductive state and the field penetration depth as the effect is lost in a quench. The critical surface of Nb3Sn is shown in Figure 2 with a reference density of 3000 A/mm^2 across the SC area selected [27, 53].

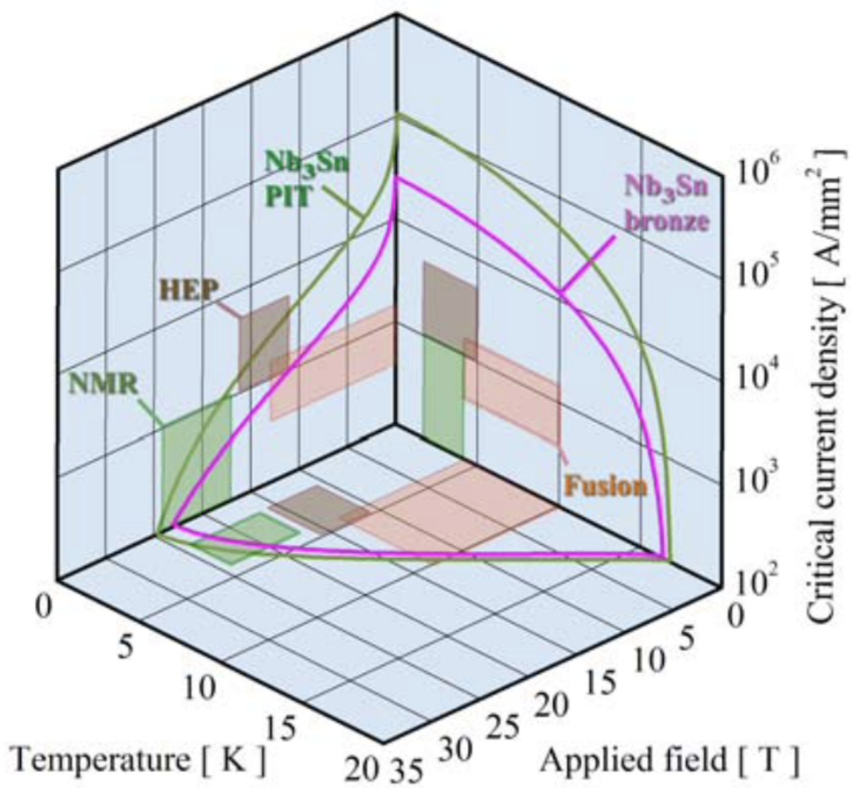

Fig. 2. Nb3Sn bounds of superconductivity

While fabrication advancements have led to the optimisation of NbTi cabling [27], the fundamental design has not changed since it's creation at the Rutherford Appleton Laboratory [36, 51]. The Rutherford cable is the most widely used cable type in accelerator magnets [26, 51]. A Rutherford cable is composed of fully transposed twisted composite strands, shown below in Figure 3 [34]. The cable critical current I_c is normally the sum of each strand's critical current [53]. The Rutherford cable is still used today because it is permeable to liquid coolants due to its braided structure and the two layers of fully transposed strands limit nonuniform current distribution within the cable, caused by the cables self field and the flux linkage between strands [51]. There are three highly stressed sections of a Rutherford cabled pulsed solenoid, the copper wire matrix around the filaments, the epoxy reinforcement and the cable (or core strip) midplane. [8, 23, 46]

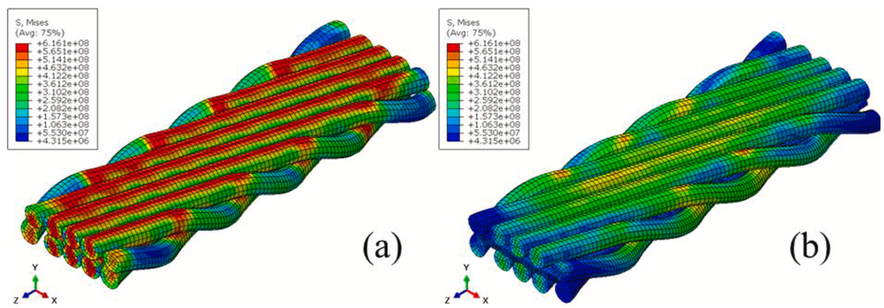

Fig. 3. Rutherford cable Von Mises stress distribution: (a) non-cored cable, (b) cored cable [34]

The feasibility of fabricating Rutherford cables with internal austenitic steel strips was demonstrated for the rapid-cycling synchrotron project at GSI [36, 60]. Austenitic steel strips provide structural reinforcement, as seen above in Figure 3, and reduces electrical losses from interstrand coupling currents. By placing a 25 micrometer thick, 8 millimeter wide austenitic steel core inside the Rutherford cables for GSI's fast-pulsed synchrotron SIS300, the cross-resistance in the cable was increased tenfold with respect to the Relativistic Heavy Ion Collider cable [59]. The ramp-rate dependence of the RHIC cable's field quality and the losses were measured at BNL [33].

Coil's designed with thinner wiring and more turns perform better analytically [52] but this results in the need for a higher voltage power supply [47]. It is more practical to use multicoil's where a number of coaxial coils are energised independently. Multicoil design is now generally accepted as the requirement for generating 80 to 100 T fields in non-destructive pulsed magnets [7, 29, 35, 56, 62] where lifetimes are in the 10,000 to 200,000 pulse range depending on configuration, field and repetition rate etc. [8]. A number of techniques can be applied to design and optimise a magnet for the intended use case, for example genetic algorithms were used to find the ideal coil configurations of the dipole magnet for the SIS300 accelerator project [41, 42].

Despite the variety of development & optimisation techniques, each design must be constructed as a finite element mesh [55] for numerical modelling. A strong coupling of field calculations, thermal simulations and analysis is presented in [2] for solenoids & in [28, 34, 58] for Rutherford windings. The thermal, electromagnetic and stress problems are solved on the same FE mesh for each step, however fine grain meshing and synergetic behaviours [25] make this approach computationally expensive [51]. The simplification of FE geometries can deliver some benefit however as the same calculations will be replicated in each satellite, an array representative of the swarm can remove detailed analysis of each element to enable reasonable run time.

With the advance of modelling tools and research, it was determined that the performance of pulsed magnets is governed by the ability of the coil materials to cope with the Lorentz forces & internal heating. The maximum field strength is limited by the power distribution busbars mechanical strength [8] while the pulse duration is limited by the power supply and heat capacity of the coil [47]. This requires a rapidly discharged power source and refrigeration system to reduce the heat generated by the intense electrical input required for each pulse. [21]. To address the thermal constraint that limits pulse duration, the use of liquid helium coolant baths is industry standard [37, 39, 31, 51]. During a pulse, coils heat up due to the large amount of electrical energy coursing through the material lattice. To cool them down again to be ready for the next pulse requires direct liquid cooling [22].

Liquid Helium is preferred for it's almost zero viscosity [57] and high specific heat capacity as a Phase II liquid when beneath 2.17K [8, 31, 51]. Beneath the phase transition surface, liquid Helium acts as a solid with almost perfect conduction. The lack of viscosity allows the liquid to fill in micrometre gaps to give complete surface coverage of the coil cabling. The removal of 'air gaps' in the cable or it's wrapped reinforcement ensures that no sites form thermal stress points for coolant boil-off and resulting quench propagation. The heat absorption capacity of the coolant bath is defined by the volume and flow rate [31] which must be balanced against the input energy joule heating of the coil [12] in line with its selected safety systems ie quench heaters. Cooling of a superconductive solenoid can thus be reduced to an energy cost based on the refrigeration & fluid control components optimised at the point of peak current in the coil, just beneath the material's quench surface.

As the optimisation of any multicoil design is strongly related to the available energy supplies for the sub-coils [48, 49] the power storage system is the final component for inspection. Given the proposed context, the highest current density will be selected before follow-on requirements are optimised. In Nb3Sn superconductors this is approximately 3000A/mm^2 thus cable wire count is defined by the maximum power supply within the available volume minus operational requirements such as cooling.

Satellite power systems have progressively shifted from nickel metal hydroxide (NiMH) to lithium-ion (Li-ion) since the early 2000s [11] and this trend is mirrored in pulsed magnetic researchers increased use of capacitor power supplied for multicoil HEPS systems as seen in [17, 18, 54, 62, 63]. A number of chemistry [6, 9, 45] and electrode options [32] are being investigated to improve existing capabilities as no transformationally new technology has commercialised successfully since Li-ion. The proposed solenoid's power system will thus be based on NiMH or Li-ion capacitors [10] as the industry standard with improvements sought from low temperature capacitor chemistries [30, 64], high current transformer input designs [3, 16] and the growing body of electric vehicle research [5].

The proposed context requires maximising mutual inductance and the peak current density, while there are many similarities to the presented accelerator electromagnet research, there are components such as the pulse transformers that will require tailored design solutions to produce an optimised pulsewave profile. The design & limits defined by this literature review are now presented in a sample coil for inspection. For the proposed coil design, resulting inductances are found and force between objects computed to determine if propulsion is viable. Analysis of this novel propulsion method uses ideal conditions that remove many of the considerations of reality, such as electrical losses or material failure modes. These initial simplifications are necessary to demonstrate the multifaceted concept is theoretically sound and analytically functional before further research and Simulink modelling can examine and document the effect of these factors in detail.

Determining Inductance

To demonstrate the concept and interactions, an iron yoked single coil solenoid of the following design is considered:

- Yoke: 99.8% Iron, Relative Permeability – u_{rs}: 5000
- Permeability of a vacuum – u_0: 4 π x 10^{-7}
- Coil wire: PIT Nb3Sn – Cored Rutherford Cable
- Wire current density capability - $\mathrm{I_s}$: 3000 A/mm^2
- Coil turn count – N_S: 200

- Coil length – l_s: 0.5 m
- Coil inner radius – a_{si}: 0.0225 m
- Coil outer radius - a_{so}: 0.0361 m
- Coil b factor – $b_s = \frac{1}{2}\, l_S = 0.25$

Inductance must be found first [52] to determine the solenoids current creation capability in the equivalent resistance circuit (ERC) of the object above, whether satellite or cargo plate, then the resultant field interaction force. If this exceeds the inertial force requirement of the proposed 2000kg freight mass then maglev cargo acceleration is a success. Inductance is a measure of influence that an electromagnetic field has on the object above's surface and to a skin penetration depth relative to the applied field strength. The field lines intersect with the conductive material and create a circular current around their intercept, the pancake coil ERC. In more conductive materials and contexts, there is a lower electrical resistance so a greater current is induced. Finding the current created in the object above's ERC is thus the key to validating the interaction.

To find the current created by the solenoid in the object above's ERC, the self inductance of each component is found then used to determine their mutual inductance as a system. Two comprehensive treatments of solenoid analysis are [52] & [31] however neither completely addresses the proposed design.

$L_s = u_0 N_s^2\ \mathrm{a}_{\text{si}}(\frac{}{2\beta})$

Solenoid self inductance [31 (3.81)] (1)

$$L_s = \frac{u_{\rho\varsigma} u_0 N_s^2\ \pi a_{\sigma\iota}^2}{}$$

englishl$_S$

Solenoid self inductance [52 (13, 21)] (2)

The self inductance formulae above do not distinguish between resistive or superconductive material selection but rather by the inclusion of a yoke rod's enhancement of the magnetic relative permeability ($u_{\text{rs}}= u_s/u_0$) in the centre of the coil and their treatment of the solenoid winding influence. The multiplicative effect of enhancing magnetic permeability within the coil's yoke rod is visible in the inductance and force generation formulae detailed in [52 (22)] and discussed further in the force derivation section below.

Magnet designers use the Fabry factors α, β to describe the solenoid shape and classify coil design subtypes [31]. The coil radii and length characteristics determine the Fabry factors and later elliptic integral results as shown below, classifying the proposed solenoid as a thin walled solenoid.

$$\alpha_s = \frac{a_{\text{so}}}{\mathrm{a}_{\text{si}}} = 1.6$$

Fabry coil design factor - Alpha [31, P115] (3)

$$\beta_s = \frac{b_s}{\mathrm{a}_{\text{si}}} = 11.1$$

Fabry coil design factor - Beta [31, P115] (4)

Equating the above self-inductance calculations to find their differences and focus on the coils alone gives the following equivalence when removing the yokes multiplicative influence:

$$\frac{\pi a_{\text{si}}^2}{l_S} \equiv a_{\text{si}} \frac{}{2\beta} = a_{\text{si}} \frac{\pi \frac{a_{\text{so}}}{\mathrm{a}_{\text{si}}}}{2 \frac{b}{\mathrm{a}_{\text{si}}}} = \frac{\pi\ \mathrm{a}_{\text{so}}\ \mathrm{a}_{\text{si}}}{l_S}$$

(1) ≡ (2) Coil design factor comparisons (5)

The reduction of the comparison above to$a_{\mathrm{si}} \equiv\ a_{\mathrm{so}}$ results in agreement of the formulae on a hypothetical coil width of zero where$a_{\mathrm{si}} =\ a_{\mathrm{so}}$. This is not unreasonable for the object above's theoretical ERC but gives an appreciable difference of 1.6 when comparing the self inductance of [52] to [31] for the tape wound solenoid. Given the latter's topic is case studies in superconductive magnet design, Iwasa's [31] formulae will be preferred. Despite this variance in the literature, it is evident that the yoke rods enhancement of magnetic permeability within a coil is a linear multiplier, though this effect diminishes and requires numerical methods once the yoke is saturated [31]. In quadrupole accelerator magnets with fields well above 1T the exterior yoke is a minor field component [31] thus the factor is actually a function and design specific modelling is required to determine the realistic effect between minor enhancement and linear multiplication. Despite this source of variance, it is clear that any conductive yoke enhances an electromagnetic field [51] thus inductance and force applied. This gives a rational basis for inclusion of u_{rs} in (1) for the proposed design despite the variance in magnitude and potential function substitution.

- (1) Solenoid Self-Inductance (S-I) - L_s: 0.0002561
- (2) Yoke Enhanced Solenoid S-I – L_s: 0.7994379
- (1+) Yoke Enhanced Solenoid S-I – L_{su}: 1.2803811

To determine the inductance of the flat metal launch plate L_P, the ERC is considered as a single wire pancake coil, acting as the second component of the two coil interaction. The proposed context can be analysed using [31 p112]'s assessment of thin solenoid to pancake coil interactions in Section 3.8.1 as there is no material specification factors between the superconductive solenoid coil or resistive metal plate.

The surficial ERC in the object above acts as a simple circuit of a single coil of wire as seen below in Figure 4. In the proposed context where a cargo plate is suspended above a square array of satellites, the voltage source represents the net effect of the induced fields. To decompose this problem, the interaction of an individual satellite's solenoid and their sub-ERC's area of effect is analysed. The inductive voltage generation and material resistance of the plate provides the inputs to resolve the circuit. The sub-ERC's and plate-wide ERC are identical, their recombination and the holistic result is discussed further below.

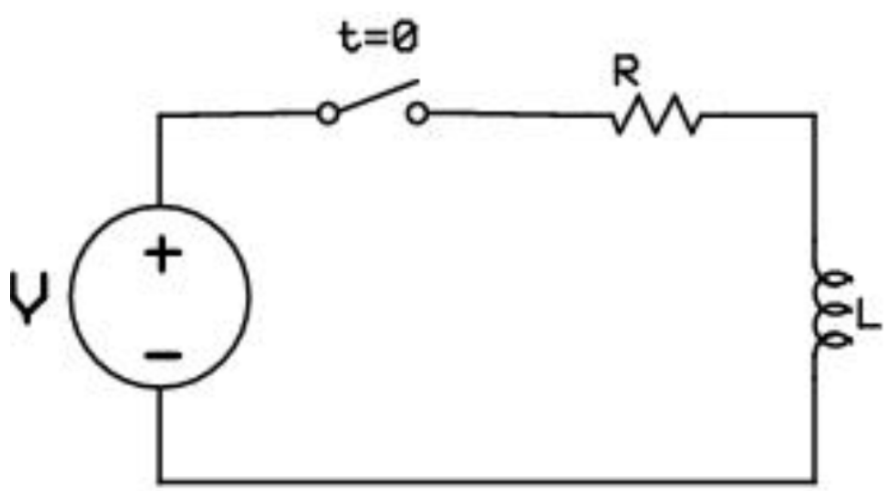

Fig. 4. Equivalent resistance circuit (ERC) [52]

Fig. 5. Thin solenoid to pancake coil interaction geometry.

To determine the Fabry factors of the sub-ERC pancake coil a theoretical wire width and coil height must be found. The square plate's overall radius, a_P, affected by each satellite, a_E, is considered geometrically at first as the length of one side divided by the number of satellites that plate edge rests upon divided in half. While there may be inductive field overlaps in reality, this theoretical division gives a bound to one satellite's area of effect and thus defines a maximum possible size of each sub-ERC. The array of values between this maximum and the minimum at $a_E = 0$ must be tested to evaluate the real intercept boundary. From the equations (1) and (3) above, it can be seen that the choice of inner radius a_{ei}, a_{pi}, has a significant effect on results by substantially increasing theα Fabry design factor at lower values. The coil height is defined by the plate thickness and can also be substituted for wire thickness for a theoretically circular wire geometry. The zero-width case is thus the local minima for calculating inductance and force generation.

- Cargo plate construction material: Steel, undefined.
- Plate Side Length: 2 m
- Supporting Satellites Per Side: 2
- Plate ERC Maximum Radius – a_{po}: 1m
- Sub-ERC Outer Radius – a_{eo}: 0.5m
- Plate Thickness - l_p: 0.05m
- Sub-ERC Inner Radius – a_{ei}: 0.45m
- Sub-ERC Fabry Factor Alpha - α_e: 1.11
- Sub-ERC Fabry Factor Beta - β_e: 0.056

Equation's (1) and (2) are specified for general solenoids while single wire pancake coils (n=1) are dependent on their α result and whether the loop is circular or rectangular in cross-section. Note$2R = a_{\mathrm{ei}}(\alpha_e + 1)$ for loop diameter &$2a = a_{\mathrm{ei}}(\alpha_e - 1)$ for loop wire diameter [31] while the permeability (non-relative) $u_e = u_p$ is defined by the cargo plates selected steel.

$L_e \cong u_0 R[\ln(\frac{R}{a}) + 0.079] + \frac{1}{4} u_e R$

Maxwell's general loop S-I (circular c-s) [31 (3.80b)] (6)

$L_e \cong u_0 R[\ln(\frac{R}{a}) + 0.886] = u_0 \frac{a_{\mathrm{ei}}(\alpha_e+1)}{2}[\ln(\frac{\frac{a_{\mathrm{ei}}(\alpha_e+1)}{2}}{\frac{a_{\mathrm{ei}}(\alpha_e-1)}{2}}) + 0.886]$

Thin ($\alpha_e \cong$1) Pancake S-I (rectangular c-s) [31 (3.86c)] (7)

$$L_e \approx \frac{1}{2} u_0 \alpha_{\mathrm{eo}} N_e^2$$

Wide ($\alpha_e \gg$1) Pancake S-I (rectangular c-s) [31 (3.86d)] (8)

- Carbon Steel, Permeability – u_{ec}: 1.26x10^{-4}
- Annealed Stainless Steel - u_{ea}: 1.26x10^{-3}
- (1) Sub-ERC Self-Inductance (S-I) – L_{e1}: 1.76x10^{-5}
- (1) Zero-width (α_e:1, β_e :0.05) - L_{e01}: 1.97x10^{-5}
- (1) Wide (α_{ei} :0.05,α_e :10, β_e :0.5) -L_{ew1}: 1.97x10^{-6}
- (6) Sub-ERC S-I (u_{ec})– L_{e6}: 1.67x10^{-5}
- (6) Sub-ERC S-I (u_{ea})– L_{e6}: 1.51x10^{-4}
- (7) Sub-ERC S-I – L_{e7}: 2.29x10^{-6}
- (6) Zero-width ERC S-I – L_{e06}: ln(x/0) t.f. null
- (7) Zero-width ERC S-I – L_{e07}: ln(x/0) 0 t.f. null
- (8) Wide ERC SI – L_{ew8}: 3.14x10^{-7}

Tabulation of formulations (1), (6), (7) & (8) allows easy comparison of self inductance values and their range. As with the earlier noted variance, it is important to understand the source of origin and the systemic effect of factor selection. Use of a low a_{ei}value is theoretically valid due to the cargo plate's homogeneous construction and this will generate a much larger alpha with an artificial inductance as the factor tends towards zero so the wide pancake case (8) is discarded for cargo plate representation. The zero width wire case is also discarded as the natural log function is not defined at zero and the cargo plate does have a conductive cross section in reality.

It must be noted again that application of the u_{re} factor to (7) would significantly change the results as seen below in (9). The result is presented as the solid metal cargo plate effectively has a large central yoke within the theoretical wire ERC thus contextually aligns with (1) & (2) as discussed above. Each formulation is calculating a result based on the coil winding geometry, primarily affect by the number of turns and the yokes enhancement of permeability when present. As such, the results of (1) are presented above before (6) & (7). Given the similarity between the geometries and results, the relative permeability u_{re} term is applied to (7) as with (1) for inspection of L_e. The resulting range of sub-ERC inductance values will later be used to calculate a minima and maxima in a range of scenarios.

$L_e \cong u_{\text{re}} u_0 R[\ln(\frac{R}{a}) + 0.886]$

Yoked Thin Pancake S-I (rectangular c-s) [31 (3.86c)] (9)

Carbon Steel Yoke Sub-ERC SI (9) – L_{e9}: 2.29x10^{-4}

Putting aside these noted sources of variance in inductance for now, to determine the induced current and resultant force pushing against the object above's inertia, the self inductances of each component must be combined to determine the two coil systems mutual inductance. The proposed single coil design is presented to remove multicoil mutual inductance calculations for clarity however the mutual inductance between each satellite's solenoid and the ERC in the object above is the key to concept validation. In coils that share a central axis, the mutual inductance M can be quickly estimated from the self inductance L and similarity of the Fabry coil design factors $\alpha\ \&\ \beta$. The k factor is an approximation from 0 to 1 of coil similarity to remove elliptic moduli as a first pass design test for easier calculation by hand [31]. Concentric coils range from k = 0.3 to 0.6 and closer to 0.6 if the Fabry factors relating coil heights and diameters are similar [31].

$$M_{\text{SP}} \equiv N_S \frac{\phi_{\text{SP}}}{I_p} \equiv M_{\text{PS}} \equiv N_p \frac{\phi_{\text{PS}}}{I_S} = k\ \sqrt{L_s L_P}$$

Mutual inductance approximation [31 (3.95a)] (10)

The detailed formulation below incorporates elliptic moduli to accurately assess the interaction between two differing winding geometries midline radius a_s & a_e (or total cargo plate radius a_p) at a distance ϱ from each other. The complete elliptical integral tables of the first K , second$E$ & third γ kind that describe the two coil systems can be seen in [31]'s Example 3.8.1 (pp. 112) and Tables 3.1 (pp. 84) & 3.2 (pp. 90) or online using the following inputs for solenoid and cargo plate sub-ERC.

$$M_{\text{se}}(\rho) = -\frac{\mu_0}{2}\left(\frac{N_s N_e}{2b_s}\right) \times$$

$$\left(\frac{\rho}{\sqrt{(a_s + a_e)^2 + \rho^2}} \begin{Bmatrix} \left[(a_s + a_e)^2 + \rho^2\right] \\ \times \left[K(k_e) - E(k_e)\right] - \gamma\left(c^2, k_e\right) \end{Bmatrix}\right.$$

$$- \frac{2b_s+\rho}{\sqrt{(a_s+ a_e)^2+ (2b_s+\rho)^2}}$$

$$\left.\begin{Bmatrix} \left[(a_s + a_e)^2 + (2b_s + \rho)^2\right] \\ \times \left[K(k_s) - E(k_s)\right] - \gamma\left(c^2, k_s\right) \end{Bmatrix}\right)$$

Mutual inductance of thin solenoid to pancake coil at distance ρ – [31 (3.98)] (11)

$$k_s = \sqrt{\frac{4a_e\ a_s}{(a_e + a_s)^2 + (2b_s + \rho)^2}}$$

Solenoid Elliptic Moduli Root [31 p112] (12)

$$k_e = \sqrt{\frac{4a_e\ a_s}{(a_e + a_s)^2 + \rho^2}}$$

Pancake Coil Elliptic Moduli Root [31 p112] (13)

$$c^2 = \frac{4a_e\ a_s}{(a_e + a_s)^2}$$

Dimensionless Elliptic Moduli [31 p112] (14)

The cargo plate rests directly on top of the satellite's as shown above in figure 5. The distance ρ between the outer edge of the solenoid and the ERC is minimal at first but increases over time as a function of the force applied and thus object acceleration.

- Solenoid midline radius - $a_s = 0.0293$m
- Sub-ERC midline radius - $a_e = 0.475$m
- Solenoid to cargo plate distance - $\rho = 0.01$m
- (12) Solenoid Elliptic Moduli – k_s: 0.32897
- (13) Sub-ERC Elliptic Moduli – k_e: 0.46777
- (14) Dimensionless Elliptic Moduli – c^2: 0.2189
- Solenoid First Elliptic Result – $K(k_s)$: 1.6161
- Sub-ERC First Elliptic Result – $K(k_e)$: 1.6692
- Solenoid Second Elliptic Result – $E(k_s)$: 1.5273
- Sub-ERC Second Elliptic Result – $E(k_e)$: 1.481
- Solenoid Third Elliptic Result –$\gamma(c^2, k_s)$: 1.8318
- Sub-ERC Third Elliptic Result – $\gamma(c^2, k_e)$: 1.8958
- (11) Mutual Inductance – $M_{\text{se}}(\rho)$: 0.00031

Mutual inductance is an independent factor relating geometries of one coil to another object in a context specific manner. In the two coil case considered there is a vacuum between the components so no $u_r$term is present to enhance the magnetic permeability of the space between the coils. The mutual inductance is purely attributed to winding geometries with no influence of current density or material selection, unlike later formulations reliant on this relationship. In superconducting quadrupoles, the mutual inductance must be tightly controlled at the design stage to prevent unintended influence in the beam control fields and is often minimised to prevent the emergence of high current segments [31]. In the proposed design context where maximising component inductance is the goal, there will be a corresponding increase in mutual inductance as seen above in (10). The result of $M_{\mathrm{se}}\left(\rho\right) = 0.00031$ presents a reasonable result for two coils of differing winding style resting on each other. The result is accepted for now until it is tested further below and the sample design is validated for the context.

The pulsed magnetic field created by each solenoid's total inductance and rapidly pulsed current determines the current induced in the surface of the object above as seen below in (15). Iwasa [31] presents the case of two separate inductively coupled superconductive coils in Problem 1.2's solution with the circuit analysis of Figure 4 shown in equation (15) below.

Once inductances are found for all components, equation (15) can be rearranged to find the pulsed time varying current induced in the plate, $\mathrm{I_P}$, in Amps per second. The traditional substitution of V=IR is not applicable in the superconductive context, giving a simplified circuit analysis despite creating a number of other concerns in reality such as the current persistence in the coil filaments. The circuit analysis result is linearly influenced by the available current in the power supply and limited by the transformer throughput to the solenoid. This reinforces the need for superconductive components with the highest current density possible to achieve peak pulse power.

$$L\frac{dI_S(t)}{\mathrm{dt}} + M_{\mathrm{SP}}\frac{dI_P(t)}{\mathrm{dt}} = 0$$

Inductively Coupled Coils [31, S1.2b] (15)

- Plate Thickness - $l_p = 0.05$m
- Circular Wire Cross Section (c-s) - $a_c = 1963.5$ mm^2
- Rectangular (Square) Wire C-S - $a_r = 2500$ mm^2

Rutherford solenoid current pulse – $I_S(t)$: 18,000 A/s Solenoid S-I Minimum (1) = 0.0002561

Sub-ERC induced current – $I_{e1}(t)$: 14,870 A/s Sub-ERC current density - I_{e1}/a_c: 7.57 A/mm^2

Rutherford solenoid current pulse – $I_S(t)$: 18,000 A/s Linearly Enhanced S-I Maximum (1) = 1.28

Sub-ERC induced current – $I_{e2}(t)$: 74,321,889 A/s Sub-ERC current density - I_{e2}/a_c: 37,851 A/mm^2

Single wire solenoid current pulse – $I_s(t)$: 3,000 A/s Solenoid S-I Minimum (1) = 0.0002561

Sub-ERC induced current – $I_{e3}(t)$: 2,478 A/s Sub-ERC current density - I_{e3}/a_c: 1.26 A/mm^2

Three scenarios presented above are inductive minimum (three) and maximum (two), combining solenoid inductance with a six wire Rutherford cable then a single Nb3Sn wire to show the variance between results for the derived calculation path. Discarding the unrealistic maximum of 74.3m A's induced in scenario two due to the engineering current density exceeding the capability of every known material, the reasonable result is between scenario one and three with the lower bound of 2,478 A/s induced in the cargo plate at the self-inductance minimum.

The standard inductance formula produce reasonable results in isolation however when applied to the proposed design generate strange outcomes which can only be assessed in verified and tested modelling tools. If the analytical path is correct, the results above may be regression tested and validated, confirming an overengineering of the proposed Rutherford cable. Scenario's one and three are accepted to follow through the force generation equation and determine a launch capability of the design. When the derivation path is calculated with $a_p$instead of $\mathrm{A_e}$, results diverge further indicating ana_x test value at a 1:1 ratio with a_s should be investigated to establish a system minima. It was highlighted above that the selection of radii for plate definition significantly affects results thus a_x is presented.

The result of testing $a_s = a_x$ is null due to the dimensionless elliptic moduli (14) being 1 and thus undefined on the chart of the third complete elliptic integral. A fractionally larger value for a_x is then considered to maintain elliptic coherency such that $a_s < a_x$. Results are presented to inspect the theoretical ERC in the object above directly opposing the solenoid.

- Solenoid midline radius - $a_s = 0.0293$m
- Sub-ERC midline radius - $a_x = 0.0294$m
- Solenoid to cargo plate distance - $\rho = 0.01$m
- Solenoid Elliptic Moduli (12) – k_s: 0.11434
- Sub-ERC Elliptic Moduli (13) – k_x: 0.98576
- Dimensionless Elliptic Moduli (14) – c^2: 0.999997
- Solenoid First Elliptic Result – $K(\ k_s)$: 1.57596
- Sub-ERC First Elliptic Result – $K(\ k_x)$: 3.1861
- Solenoid Second Elliptic Result – $E(\ k_s)$: 1.5656
- Sub-ERC Second Elliptic Result – $E(\ k_x)$: 1.03797
- Solenoid Third Elliptic Result –$\gamma(\ c^2, k_s)$: 912.87
- Sub-ERC Third Elliptic Result – $\gamma(\ c^2, k_x)$: 5367.32
- Mutual Inductance – $M_{\mathrm{sx}}(\rho)$: 0.001383
- Scenario 1 sub-ERC induced current – I_{x1}: 3,333 A/s
- Scenario 1 current density - I_{x1}/a_c: 1.70 A/mm^2
- Scenario 3 sub-ERC induced current – I_{x3}: 555 A/s
- Scenario 3 current density - I_{x3}/a_c: 0.28 A/mm^2

At this stage, it is unclear whether results are unrealistic from a foundational error present in formulation or analysis, or if by absence of error, the derivation path is correct. Scenario's one and three produce valid current densities across a range of cargo plate radii so their force application must be examined.

Applied Force Derivation

[I] is a case study in superconductive magnet design and details the interaction of superconductor's winding style to create self-inductance, then in multiple 2-coil system design contexts but without the presence of yoke rods. [31]'s Example 3.5.3 below is an analytical formulation of the proposed design context and uses only u_0 for calculating force as a result of inductance as the two coils in the interaction are considered only in relation to each other in a vacuum. [52] addresses the single solenoid context and includes the linear enhancement of the force by the yokes relative permeability $u_r$which was demonstrated as nonrelevant from scenario one above. [52]'s formulae for force interaction include the term but are reliant on a materials resistance, which does not address the superconductive context of R = 0. Despite this, the potential enhancement effect of the yoke rod is again noted though not included, unlike above.

[31]'s Example 3.5.3 illustrates the force experienced at the top of an unyoked coil in a long thin solenoid when acting against the pancake coil. That force derivation is shown below utilising the inductance and current inputs to scenario one and three above.

$$F_{\mathrm{sz}}(\rho) = -\frac{\mu_0}{2}\left(N_e I_e\right)\left(\frac{N_s I_s}{2b_s}\right) \times$$

$$(\ \sqrt{\left(a_s + a_e\right)^2 + \left(2b_s + \rho\right)^2}\ \left\{\begin{matrix} 2\left[K\left(k_s\right) - E\left(k_s\right)\right] \\ -k_s^2 K\left(k_s\right) \end{matrix}\right\}$$

$$- \sqrt{\left(a_s + a_e\right)^2 + \rho^2}\ \left\{2\left[K\left(k_e\right) - E\left(k_e\right)\right] - k_e^2 K\left(k_e\right)\right\}\ )$$

Force acting against a solenoid end in z [31 (3.42)] (17)

The results required in (17) include k^2 terms but all moduli are identical to the earlier mutual inductance moduli (12,13) across the various scenarios with results from the same tables of complete elliptic integrals.

- Scenario $1a_e$ sub-ERC current – I_{e1}: 14,870 A/s
- Scenario $1a_e$ force - $F_{e1}(\rho) = 293$ N
- Scenario $1a_x$ sub-ERC current – I_{x1}: 3,333 A/s
- Scenario $1a_x$ force - $F_{x1}(\rho) = 1076$ N
- Scenario $3a_e$ sub-ERC current – I_{e3}: 2,478 A/s
- Scenario $3a_e$ force - $F_{e3}(\rho) = 8.16$ N
- Scenario $3a_x$ sub-ERC current – I_{x3}: 555 A/s
- Scenario $3a_x$ force - $F_{x3}(\rho) = 29.9$ N

As scenario $1a_e$ has a current density of 7.57 A/mm^2 there will be a reduction in solenoid current required to ensure the selected plate steel is able to handle the induced current. Scenario $1a_x$ is the clear preference given the highest newton force generated, corresponding to the highest current in the smallest ERC size. As with results above, the presented results are for a single coil solenoid to a sub-ERC within the object above so a number of factors such as coil count and yoke enhancement may be applied to alter results further. It is noted that the larger the ERC, the higher the current and the lower the corresponding force generation. As the design context proposed is a square array of four satellites under the cargo plate, the force result can potentially be combined linearly for first pass analysis however as demonstrated above it can be seen that mutual inductances between the sub-ERC's will have an effect. Interestingly the results of scenario's $1a_e$ and $1a_x$demonstrate that the six wire Rutherford cabling gives a linear multiple of induced current compared to the single wire scenario's $3a_e$ and $3a_x$while the force generated increases by 36 times, or six squared.

This final observation gives strong evidence for the use of Rutherford cabled solenoids in the proposed design context. The use of a yoked dual coil design with a correspondingly high total inductance between all subcomponents will thus produce the optimal result despite the variances noted in ERC radii. Simulink modelling is a clear necessity to determine accurate electromagnetic field intercepts and ERC definition due to the noted sources of variance. The results will be accepted for now and inspected following definition of the cargo acceleration success criterion.

Success Criterion Isolation

The force experienced at the top of the solenoid relative to the plate distance of ρ is created by the interaction of the pulsed and the induced electromagnetic fields. This force is acting on both the solenoid top and the surficial ERC in the under-side of the object above. The force must exceed the inertia of the object above to create maglev thrust and initiate propulsion. Any object's inertia is a product of the mass and change in acceleration or local gravity. In orbit, a degree of gravity is present, anchoring satellites and the moon to their respective orbits. To determine the contextual object above's inertia, the standard G = 9.8 m/s^2 is used to generate the upper bound value for force required to move that object from it's resting orbit.

With the inertial force for a chosen mass and gravity set as the left hand side of (17) and all other factors except the currents $I_s$and $I_{e/p}$ being determined by coil winding geometry, the equation can be simplified to optimise the power supply system. The reduction of all coil design and resulting elliptical factors into a single multiplier of the plates induced current I_P allows designs to be quickly inspected for validity in the same manner as (10) above. Any inertial force requirement can be set then a required current found for comparison to the induced current, if the induced current is larger than that required, maglev propulsion is a success. Alternatively, if the induced current far exceeds the required current, (18) could be rearranged to find the largest accelerable mass for any design. The derivation path is applicable to any two coil context however the interaction formulae do change based on winding geometry categories.

$$F_{\mathrm{sz}}(\rho) = \ \varpi \ I_P = \ \frac{\mathrm{L}\ \frac{dI_S(t)}{\mathrm{dt}}}{M} = ma = \ F_{\mathrm{ma}}$$

Magnetic force interaction simplification (18)

The satellite propelled cargo containers will be accelerated at tiered rates according to their contents. Construction materials and non-sensitive bulk cargo could potentially be launched at up to 50 G pulsed acceleration however sensitive equipment will be limited to 20 G acceleration change in line with NASA's 2018 Mars Rover orbital entry speed.

- Cargo mass – m_c = 2,000 kg
- Gravity Constant – G = 9.8 m/s^2
- 20 G Acceleration – a_{20} = 196 m/s^2
- 50 G Acceleration – a_{50} = 490 m/s^2
- Scenario F_{c20} Force - 20 G for 1 s = 392 kN
- Scenario F_{c50} Force - 50 G for 1 s = 980 kN
- Carbon steel density = 7.85 g/cm^3
- Cargo plate mass - m_p = 1,570 kg
- Total object mass - m_t = 3,570 kg
- Scenario F_{t20} Force - 20 G for 1 s = 700 kN
- Scenario F_{t50} Force - 50 G for 1 s = 1,749 kN

While the scenarios above discuss a steel plate's decomposition for electromagnetic analysis, from the presented dimensions the calculated mass exceeds that of a 20-ft shipping container with a cargo mass capacity of 25,400 kg. This leads to the conclusion that a variety of container designs can be substituted within that representative plate mass m_p and then optimised to achieve success. To assess the viability of the overall system, both the cargo mass m_c and container mass m_p must be totalled m_t then later optimised with respect to the solenoid strength and power storage capacity.

To accelerate the proposed cargo and plate at 50 G for a 1 second pulse requires a force F_{t50} of 1749 kN to overcome inertia whileF_{c20} = 392 kN is the local minima at 22% of F_{t50}. Considered in reverse, F_{t50} is 446% of F_{c20} resulting from the 178.5% increase from m_c to m_t and increase of acceleration by 250% from 20G to 50G. With the force requirement being met by a sum of propulsion pulse vectors, the required force output per individual satellite is lower however the composition of this function must be investigated specifically due to the multitude of mutual inductances. Swarm force distribution function aside, achieving the minima of 392 kN force in F_{c20} for scenario $1a_e$ requires a pulse induced current I_{1e} of 23.5x10^6 A andI_{1x} of 1.2x10^6 A when considering the minimum ERC scenario $1a_x$. While the peak current and minimum ERC size scenario is optimal, no presented scenario achieved the required current induction for successful maglev propulsion. Division of the induction requirement between four tethered satellites under the plate does not achieve the requisite current with the presented design either. Despite this, the investigation of the problem context and construction delivered valuable design conclusions.

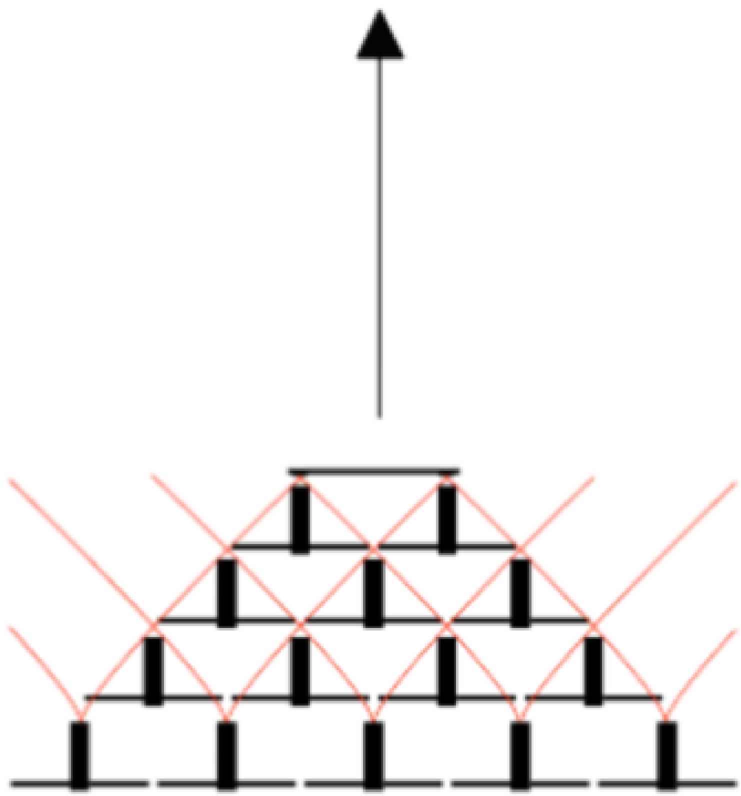

Fig. 6. Generalised Solenoid To Object Above Pulse Interaction In ZX & ZY Planar View.

Conclusions

The derived success criterion based on the induced current provides clear results for design assessment. The analysis path is applicable to any two coil context provided the appropriate winding geometry substitutions are made. This leads to the conclusion that the paper's objective of isolating a general success criterion is achieved despite no presented scenario being successful in achieving propulsion.

Discussion of the presented scenarios is able to inform future design thinking to prioritise solenoid inductivity, coil width and current carrying capacity to generate the maximum force and overcome any conductive object above's inertia. Further investigation of multicoil solenoids and cargo plate design is suggested as the solution to creating a successful scenario. The noted sources of variance in electromagnetic results from plate decomposition to theoretical ERC's is an area suggested for significant research to resolve the presented complexities in an analytical manner without resorting to finite element methods.

These challenges can be addressed with the application of numerical methods in industry verified FEM software such as MATLAB's Simulink multiphysics suite however all models are still reliant on the validity of their base assumptions. Thus the investigation of geometry to frame this problem and bound it with current material limits and design thinking is the key to constructing a valid model.

In summary, solenoid coil design determines inductance, which is assessed against stored power to determine the induced current and resultant repulsion force required to overcome an object above's inertia. The proposed propulsion method combines multiple maglev propulsion vectors to reduce the requirements on individual satellites and must be investigated with numerical methods. The swarm satellite application of high energy pulsed solenoids in freight transport is a new use case for both technologies. It is proposed here for peer review and to initiate further research on design and componentry.

Reaching Mars is achievable today with our current technology, the only barrier to entry is cost. Just as reusable rocket systems are drastically reducing the cost of orbital entry, mass produced, reusable, interorbital freight transport satellite swarms could drive down the cost of freight crossing the void. Establishment of freight shipping lanes between orbits will be the connector that enables crewed missions to commence safely and provide the ongoing support required for humanity to become an interplanetary species.

References

1. D. Aguglia, J. Cravero, R. Rebeschini, S. Iovieno & C. Russo, "Design solutions for compact high current pulse transformers for particle accelerators' magnet powering," CERN, Geneva, Switzerland, October 2015. DOI: CERN-ACC-2015-0105
2. G. Aird, J. Simkin, S. Taylor, C. Trowbridge & E. Xu. "Coupled transient thermal and electromagnetic finite element simulation of quench in superconducting magnets." in Proceedings of ICAP, Chamonix, France, October 2006, pp. 70-73, DOI: MOAPMP01
3. A. Algarni, F. Gleason, & A. Mohanakumaran, "Electromagnetic ring launcher," WPI, Worcester, England, 2014. DOI: E-project-050114-192748
4. A. Ali, L. M. Reyneri, H. Ali & M. Rizwan Mughal, "Components selection for a simple boost converter on the basis of power loss analysis," in *63rd International Astronautical Congress* , pp. 1–5, Naples, Italy, October 2012. DOI: IAC-12-C3.4.3
5. M. Al Sakka, H. Gualous, J. Van Mierlo & H. Culcu. "Thermal modeling and heat management of supercapacitor modules for vehicle applications." Journal of Power Sources, 2009, vol. 194, no. 2, pp. 581–587, DOI: 10.1016/j.jpowsour.2009.06.038
6. M. Anouti, E. Couadou, L. Timperman & H. Galiano, "Protic ionic liquid as electrolyte for high-densities electrochemical double layer capacitors with activated carbon electrode material." in*Electrochimica Acta* , vol. 64, pp. 110-117, March 2012, DOI: 10.1016/j.electacta.2011.12.120
7. J. Bacon, C. Ammerman, H. Coe, G. Ellis, B. Lesch, J. Sims, J. Schillig & C. Swenson, "The US NHMFL 100 Tesla multishot magnet." in IEEE Transactions on Applied Superconductivity, vol. 12, no. 1, pp. 695-698, March 2002, DOI: 10.1109/TASC.2002.1018496
8. M. D. Bird, A. V. Gavrilin, S. R. Gundlach, K. Han, C. A. Swenson and Y. M. Eyssa, "Design & Testing of a Repetitively Pulsed Magnet for Neutron Scattering," in IEEE Transactions on Applied Superconductivity, vol. 16, no. 2, pp. 1676-1679, June 2006, DOI: 10.1109/TASC.2006.870841.
9. F. Boattini & C. Genton, "Accelerated lifetime testing of energy storage capacitors used in particle accelerator power converters." at EPE'15 ECCE-Europe, September 2015, DOI: 10.1109/EPE.2015.7309424
10. Y. Borthomieu, D. Prevot, J. Massot, P. Tastet & E. Simon, "VES100/140 Lithium-Ion Cells LEO Life-Test Results & Proteus Flight Heritage." in Proceedings of the 9th European Space Power Conference, ESPC 2011, Saint Raphael, France, vol. 690, October 2011. DOI: 2011ESASP.690E..94B
11. Y. Borthomieu, "Satellite Lithium-Ion Batteries." Saft, Defence and Space Division, Poitiers Cedex, France, January 2014. DOI: 10.1016/B978-0-444-59513-3.00014-5
12. A. V. Bragin, S. V. Khrushchev, V. V. Kubarev, N. A. Mezencev, V. M. Tsukanov, G. I. Sozinov & V. A. Shkaruba, "Superconducting solenoid for superfast Thz spectroscopy." in *Physics Procedia* , vol. 84, pp. 84-85, December 2016. DOI: 10.1016/j.phpro.2016.11.014
13. B. Brandt, S. Hannahs, H. Schneider-Muntau, G. Boebinger & N. Sullivan, "The national high magnetic field laboratory." in*Physica B Condensed Matter* , vol. 294, pp. 505-511, January 2001. DOI:

10.1016/S0921-4526(00)00711-0
14. W. Brunk & D. Walz, “A new pulse magnet design utilising tape wound cores.” in *IEEE Transactions on Nuclear Science* , vol. 22, no. 3, pp. 1548-1551, July 1975. DOI: 10.1109/TNS.1975.4327931
15. A. F. Castric, S. Lawson & Y. Borthomieu, “High energy lithium-ion VES cells and batteries performance.” in Proceedings of the 9th European Space Power Conference, Saint Raphael, France, vol. 690, pp. 1-8, October 2011. DOI: 978-92-9092-257-5
16. J. Cravero, G. Maire & J. Royer, “High current capacitor discharge power converters for the magnetic lenses of a neutrino beam facility.” in 2007 European Conference on Power Electronics and Applications, pp. 1-8, October 2007. DOI: 10.1109/EPE.2007.4417351
17. H. Ding, T. Ding, C. Jiang, Y. Xu, H. Xiao, L. Li, X. Duan & Y. Pan, “Design of Power Supplies for the Pulsed High Magnetic Field Facility at HUST.” in *Journal of Low Temperature Physics* , vol. 159, no. 1, pp. 349-353, April 2010. DOI: 10.1007/s10909-009-0135-1
18. H. Ding, X. Jiang, T. Ding, Y. Xu, L. Li, X. Duan, Y. Pan & F. Herlach, “Prototype test and manufacture of a modular 12.5 MJ capacitive pulsed power supply.” in *IEEE Transactions on Applied Superconductivity* , vol. 20, no. 3, pp. 1676-1680, June 2010. DOI: 10.1109/TASC.2009.2039785
19. H. Ding, J. Hu, W. Liu, Y. Xu, C. Jiang, T. Ding, D. Xianzhong & Y. Pan, “Design of a 135 MW Power Supply for a 50 T Pulsed Magnet.” in*IEEE Transactions on Applied Superconductivity* , vol. 22, no.3, pp. 5400504-5400504, June 2012. DOI: 10.1109/TASC.2012.2183630
20. H. Ding, T. Ren, Y. Xu, T. Ding, Z. Zhao, T. Peng, L. Li & J. Hu, “Design and analysis of power supplies for the first 100T nondestructive magnet at the WHMFC,” in *IEEE Transactions on Applied Superconductivity* , vol. 26, no. 4, pp. 1-5, June 2016, DOI: 10.1109/ TASC.2016.2531793.
21. H. Ding, Z. Zhao, C. Jiang, Y. Xu, T. Ding, X. Fang, T. Ren, L. Li, Y. Pan, T. Peng, ”Construction and Test of Three-Coil Magnet Power Supply System for a High-Pulsed Magnetic Field,” in *IEEE Transactions on Applied Superconductivity* , vol. 28, no. 3, pp. 1-6, Apr. 2018. DOI: 10.1109/TASC.2018.2801830.
22. Y. Eyssa, R. Walsh, J. Miller, P. Pernambuco-Wise, M. Bird & H. Schneider-Muntau, “2 Hz, 30 T Split Pulse Water Cooled Magnet for Neutron Scattering Experiments.” National High Magnetic Field Laboratory Technical Report, no. LA-SUB-00-47, August 1997. DOI: 10.2172/760057
23. Y. Eyssa, R. Walsh, J. Miller, P. Pernambuco-Wise, M. Bird, H. Schneider-Muntau, H. Boeing & R. Robinson, ”25-30T water cooled pulsed magnet concept for neutron scattering experiment.” in Proc. of the 15th Int. Conf. on Magnet Technology pp. 691–694, Science Press. Beijing, China, December 1997. DOI: LA-UR-97-4477; CONF-9710127-ON: DE98002925
24. C. Fahrni, A. Rufer, F. Bordry and J. Burnet, ”A novel 60 MW pulsed power system based on capacitive energy storage for particle accelerators,” 2007 European Conference on Power Electronics and Applications, pp. 1-10, 2007, DOI: 10.1109/ EPE.2007.4417398.
25. R. B. Fuller, “Synergetics: Explorations in the geometry of thinking.” New York, USA, Macmillan, 1975. DOI: 978-0020653202
26. G. Gallagher-Daggit, “Superconductor cables for pulsed dipole magnets.” Rutherford High Energy Laboratory Memorandum, no. RHEL/M/A25, Chilton, Didcot, 1973. DOI: RHEL/M/A25 - 21090
27. A. Godeke, “Performance boundaries of Nb3Sn superconductors”, PhD Thesis Univ. of Twente, Enschede, The Netherlands, 2005. DOI: ISBN 90-365-2224-2
28. P. P. Granieri, M. Calvi, P. Xydi, B. Baudouy, D. Bocian, L. Bottura, M. Breshi & A. Seikmo, “Stability analysis of the LHC cables for transient heat depositions.” in *IEEE Transactions on Applied Superconductivity* , vol. 18, no. 2, pp. 1257-1262, July 2008. DOI: 10.1109/TASC.2008.922543
29. K. Han, A. Ishmaku, Y. Xin, H. Garmestani, V. Toplosky, R. Walsh, C. Swenson, B. Lesch, H. Ledbetter, S. Kim, M. Hundley & J. Sims, “Mechanical properties of MP35N as a reinforcement material for pulsed magnets.” in *IEEE Transactions on Applied Superconductivity* , vol. 12, no. 1, pp. 1244-1247, April 2002. DOI: 10.1109/TASC.2002.1018627
30. K. Hung, C. Masarapu, T. Ko & B. Wei, “Wide-temperature Range Operation Supercapacitors From Nanostructured Activated Carbon Fabric.” in *Journal of Power Sources* , vol. 193, no. 2, pp. 944-949, September 2009. DOI: 10.1016/j.jpowsour.2009.01.083

31. Y. Iwasa, “Case Studies In Superconducting Magnets,” 2nd ed., New York, NY, USA, Springer, pp. 1-112. 2009. DOI: 10.1007/b112047
32. A. Izadi-Najafabadi, S. Yasuda, K. Kobashi, T. Yamada, D. Futaba, H. Hatori, M. Yumura, S. Ilijima & K. Hata, “Extracting The Full Potential Of Single-Waller Carbon Nanotubes As Durable Supercapacitor Electrodes Operable At 4V With High Power And Energy Density.” in *Journal of Advanced Materials* , vol. 22, no. 35, pp. 235-41, September 2010. DOI: 10.1002/adma.200904349
33. A. Jain, G. Ganetis, A. Gosh, L. Wing, A. Marone, R. Thomas & P. Wanderer, “Field quality measurements at high ramp rates in a prototype dipole for the FAIR project.” in *IEEE Transactions on Applied Superconductivity* , vol. 18, no. 2, pp. 1629-1632, July 2008. DOI: 10.1109/TASC.2008.921219
34. L. Jiang, J. Zhao, Y. Gao & Y. Zhou, “Geometrical modelling and mechanical behaviour analysis of Nb3Sn Rutherford cable.” in *Cryogenics* , vol. 119, no. 103361, pp. 1-10, September 2021. DOI: 10.1016/j.cryogenics.2021.103361
35. H. Jones, P. Frings, M. von Ortenberg, A. Lagutin, L. van Bockstal, O. Portugall & F. Herlach, “First experiments in fields about 75T in the European “coilin - coilex” magnet.” in *Physica B Condensed Matter* , vol. 346, no. 1, pp. 553-560, April 2004. DOI: 10.1016/j.physb.2004.01.081
36. J. Kaugerts, G. Moritz, C. Muehle, A. Ageev, I. O. Bogdanov, S. Kozub, P. Shcherbakov, V. Sytnik, L. Tkachenko, V. Zubko, D. Tommasini, M. Wilson & W. Hassenzahl, “Design of a 6T, 1 T/s fast-ramping synchrotron magnet for GSIs planned SIS300 Accelerator.” in *IEEE Transactions on Applied Superconductivity* , vol. 15, no. 2, pp. 1225-1227, June 2005. DOI: 10.1109/TASC.2005.849537
37. M. Kauschke & C. H. Schroeder, “Cryogenic system for the new international accelerator facility for research with ions and antiprotons at GSI,” Adv. Cryogenic Eng., vol. 49 A, pp. 363–370, June 2004. DOI: 10.1063/1.1774704
38. M. Khan, A. Ali, H. Ali, M. Khattak & I. Ahmad, “Designing Efficient Electric Power Supply System for Micro-Satellite.” in *2016 International Conference on Computing, Electronic and Electrical Engineering* , (ICE Cube), pp. 207-212, April 2016. DOI: 10.1109/ICECUBE.2016.7495225
39. P. Lebrun, “Advanced technology from and for basic science: superconductivity and superfluid helium at the large hadron collider, CERN.” in *European Centre for Nuclear Research Departmental Report* , January 2007. DOI: CERN/AT 2007-30
40. W. S. Marshall, C. A. Swenson, A. V. Gavrilin, & H. J. Schneider-Muntau, “Development of ‘Fast Cool’ pulsed magnet coil technology at NHMFL.” in *Physica B Condensed Matter* vol. 346, pp. 594–598, 2004. DOI: 10.1016/j.physb.2004.01.156
41. G. Moritz, “Fast-pulsed SC magnets.” in *Proceedings of European Particle Accelerator Conference, EPAC* , Lucerne, Switzerland, pp. 132-136, July 2004. DOI: 92-9083-231-2
42. G. Moritz, C. Muehle, M. Anerella, A. Ghosh, W. Sampson, P. Wanderer, E. Willen, N. Agapov, H. Khodzhibagiyan, A. Kovalenko, W. Hassenzahl & M. N. Wilson, “Towards fast pulsed superconducting synchrotron magnets.” PACS2001. Proceedings of the Particle Accelerator Conference, February 2001, pp. 211-213. DOI: 10.1109/PAC.2001.987472
43. M. Motokawa, H. Hojiri, J. Ishihara & K. Ohnishi, “Production of repeating pulsed high magnetic field.” in Physica B Condensed Matter, vol. 155, no. 1, pp. 39-42. March 1989. DOI: 10.1016/0921-4526(89)90458-4
44. H. Nojiri, M. Motokawa, K. Takahashi & M. Arai, “30 T repeating pulsed field system for neutron diffraction.” in *IEEE Transactions on Applied Superconductivity* , vol. 10, no. 1, pp. 534-537, April 2000. DOI: 10.1109/77.828290
45. K. A. O’Connor & R. D. Curry, “Recent Results in the Development of composites for High Energy Density Capacitors.” in 2014 IEEE International Power Modulator and High Voltage Conference (IPMHVC), pp. 496-499 October 2015. DOI: 10.1109/IPMHVC.2014.7287320
46. T. Painter, S. Bole, Y. Eyssa, I. Dixon, V. Williams, S. Maier, S. Gundlach, S. Tozer, Y. Hascicek & C. Ammerman, “Design of 30 T split pair pulse coils for LANSCE.” in *IEEE Transactions on Applied Superconductivity* , vol. 10, no. 1, pp. 538-541, April 2000. DOI: 10.1109/77.828291
47. T. Peng & F. Herlach, “Design Principles for Optimised Pulsed Magnets.” *2008 International Conference on Electrical Machines and Systems, ICEMS 2008,* Wuhan, China, pp. 679-684. DOI: 978-1-

4244-3826-6
48. T. Peng, L. Li, J. Vanacken & F. Herlach, "Efficient Design of Advanced Pulsed Magnets." in *IEEE Transactions on Applied Superconductivity* , vol. 18, no. 2, pp. 1509-1512, June 2008. DOI: 10.1109/TASC.2008.921300.
49. J. Perenboom, P. Frings, J. Beard, B. Bansai, F. Herlach, T. Peng & S. Zherlitsyn, "Optimisation of large multiple coil systems for pulsed magnets." in Journal of Low Temperature Physics vol. 159, no. 1, pp. 336-340, April 2010. DOI: 10.1007/s10909-009-0137-z
50. L. V. Potanina, A. K. Shikov, A. E. Vorobieva, N. I. Salunin, M. I. Medvedev, V. E. Keilin, I. A. Kovalev & S. L. Kruglov, "Nb3SN And NbTi Multifilamentary Wires With Enhanced Heat Capacity." in AIP Conference Proceedings vol. 986, pp. 349, March 2008, DOI: 10.1063/1.2900366
51. S. Russenschuck, "Field Computation for Accelerator Magnets." Weinheim, Germany, Wiley, pp. 1-48, Jan. 2010. DOI: 10.1002/9783527635467
52. P. H. Schimpf, "A detailed explanation of solenoid force," in*Int. J. on Recent Trends in Engineering and Technology* , vol. 8, no. 2, pp. 7-14, Jan. 2013. DOI: 01.IJRTET.8.2.25
53. D. Schoerling & A. V. Zlobin, "Nb3Sn Accelerator Magnets - Designs, Technologies and Performance." CERN, Switzerland, Springer, pp. 23-51, 2019. DOI: 10.1007/978-3-030-16118-7
54. J. Shi, X. Han, J. Xie & L. Li, "Analysis and Design of a Control System for the 100T Pulsed High Magnetic Field Facility at WHMFC." in*IEEE Transactions on Applied Superconductivity* , vol. 24, no. 6, pp. x, June 2016. DOI: 10.1109/TASC.2016.2517245
55. Y. Skourski, T. Herrmannsdorfer A. Sytcheva, J. Wosnitza, B. Wustmann & S. Zherlitsyn, "Finite element simulation and performance of pulsed magnets." in *IEEE Transactions on Applied Superconductivity* , vol. 18, no. 2, pp. 608-611, June 2008, DOI: 10.1109/TASC.2008.922286.
56. C. A. Swenson, W. S. Marshall, A. V. Gavrilin, K. Han, J. Schillig, J. R. Sims & H. J. Schneider-Muntau, "Progress of the insert coil for the US-NHMFL 100 T multi-shot pulse magnet." in *Physica B Condensed Matter,* vol. 346, pp. 561-565, April 2004, DOI: 10.1016/j.physb.2004.01.082
57. D. R. Tilley & J. Tilley, "Superfluidity and Superconductivity." New York, USA, Routledge, pp. 1-30, 1990. DOI: 10.1201/9780203737897
58. A. Verweij, "CUDI: A model for Calculation of Electrodynamic and Thermal Behaviour of Superconducting Rutherford Cables." in*Journal of Cryogenics,* Vol. 46 No. 7, pp. 619-626, July 2006. DOI: 10.1016/j.cryogenics.2006.01.009
59. P. Wanderer, M. Anerella, G. Ganetis, A. Ghosh, P. Joshi, A. Marone, J. Muratore, J. Schmalle, R. Soika, R. Thomas, J. Kaugerts, G. Moritz, W. Hessenzahl & M. Wilson, "Initial test of a fast-ramped superconducting model dipole for GSIs proposed SIS200 accelerator." in *Proceedings of the Particle Accelerator Conference, 2003.*vol. 4, pp. 2162-2164, DOI: 10.1109/PAC.2003.1289052
60. M. N. Wilson, A. Ghosh, B. Ten Haken, W. Hassenzahl, J. Kaugerts, G. Moritz, C. Muehle, A. Den Ouden, R. Soika, P. Wanderer & W. Wessel, "Cored Rutherford cables for the GSI fast-ramping synchrotron." in*IEEE Transactions on Applied Superconductivity* , vol. 13, no. 2, pp. 1704-1709, June 2003. DOI: 10.1109/TASC.2003.812864
61. M. N. Wilson, "100 years of superconductivity and 50 years of superconducting magnets." in *IEEE Transactions on Applied Superconductivity* , vol. 22 no. 3, pp. 3800212-3800224, June 2012. DOI: 10.1109/TASC.2011.2174628
62. S. Zherlitsyn, T. Herrmannsdorfer, B. Wurstmann & J. Wosnitza, "Design and performance of nondestructive pulsed magnets at the Dresden High Magnetic Field Laboratory." in *IEEE Transactions on Applied Superconductivity,* vol. 20, no. 3, pp. 672-675, Jun. 2010. DOI: 10.1109/TASC.2010.2044158
63. J. Zhou, H. Ding, Y. Liu, Z. Zhao, Y. Huang, X. Fang & Q. Wang, "A High Power Charging Power Supply For Capacitor in Pulsed Power System." in IEEE 21st International Conference on Pulsed Power (PPC), 2017, pp. 1-4, June 2017. DOI: 10.1109/PPC.2017.8291222
64. Y. Zhou, M. Ghaffari, M. Lin, H. Xu, H. Xie, C. M. Koo & M. Zhang. "High performance supercapacitor under extremely low environmental temperature." *RSC Adv.,* vol. 5, pp. 71699-71703, Aug. 2015. DOI: 10.1039/C5RA14016A